Ultrasound in Med. & Biol., Vol. 34, No. 10, pp. 1578–1589, 2008

0301-5629/08/$–see front matter

ELSEVIER

doi:10.1016/j.ultrasmedbio.2008.02.012

● *Original Contribution*

CHARACTERIZATION OF ULTRASOUND PROPAGATION THROUGH *EX VIVO* HUMAN TEMPORAL BONE

AZZDINE Y. AMMI,* T. DOUGLAS MAST,* I-HUA HUANG,§ TODD A. ABRUZZO,§* CONSTANTIN-C. COUSSIOS,† GEORGE J. SHAW,*‡ and CHRISTY K. HOLLAND*§

*Department of Biomedical Engineering, University of Cincinnati, Cincinnati, OH, USA; †Department of Engineering Science, Institute of Biomedical Engineering, Oxford, UK; and ‡Departments of Emergency Medicine and §Radiology, University of Cincinnati, Cincinnati, OH, USA

(*Received* 26 *September* 2007; *revised* 14 *December* 2007; *in final form* 5 *February* 2008)

Abstract—Adjuvant therapies that lower the thrombolytic dose or increase its efficacy would represent a significant breakthrough in the treatment of patients with ischemic stroke. The objective of this study was to perform intracranial measurements of the acoustic pressure field generated by 0.12, 1.03 and 2.00-MHz ultrasound transducers to identify optimal ultrasound parameters that would maximize penetration and minimize aberration of the beam. To achieve this goal, *in vitro* experiments were conducted on five human skull specimens. In a water-filled tank, two unfocused transducers (0.12 and 1.03 MHz) and one focused transducer (2.00 MHz) were consecutively placed near the right temporal bone of each skull. A hydrophone, mounted on a micropositioning system, was moved to an estimated location of the middle cerebral artery (MCA) origin, and measurements of the surrounding acoustic pressure field were performed. For each measurement, the distance from the position of maximum acoustic pressure to the estimated origin of the MCA inside the skulls was quantified. The −3 dB depth-of-field and beamwidth in the skull were also investigated as a function of the three frequencies. Results show that the transducer alignment relative to the skull is a significant determinant of the detailed behavior of the acoustic field inside the skull. For optimal penetration, insonation normal to the temporal bone was needed. The shape of the 0.12-MHz intracranial beam was more distorted than those at 1.03 and 2.00 MHz because of the large aperture and beamwidth. However, lower ultrasound pressure reduction was observed at 0.12 MHz (22.5%). At 1.03 and 2.00 MHz, two skulls had an insufficient temporal bone window and attenuated the beam severely (up to 96.6% pressure reduction). For all frequencies, constructive and destructive interference patterns were seen near the contralateral skull wall at various elevations. The 0.12-MHz ultrasound beam depth-of-field was affected the most when passing through the temporal bone and showed a decrease in size of more than 55% on average. The speed of sound in the temporal bone of each skull was estimated at 1.03 MHz and demonstrated a large range (1752.1 to 3285.3 m/s). Attenuation coefficients at 1.03 and 2.00 MHz were also derived for each of the five skull specimens. This work provides needed information on ultrasound beam shapes inside the human skull, which is a necessary first step for the development of an optimal transcranial ultrasound–enhanced thrombolysis device. (E-mail: Christy.Holland@uc.edu)

Key Words: **Intracranial ultrasound, Transcranial ultrasound, Ultrasound-enhanced thrombolysis, Temporal bone window insufficiency, Ultrasound of the brain, Neurosonography.**

INTRODUCTION

Acute ischemic strokes are the result of a partial or complete occlusion of a brain artery, commonly the middle cerebral artery (MCA), by a thrombus or embolus (Zhil'tsova 1965; Toumanidis 1995; Marder et al. 2006). This artery carries the majority of the blood flow to each hemisphere. Many thrombolytic agents have been investigated for their efficacy (*e.g.*, urokinase, streptokinase, *etc.*) (Berg-Dammer et al. 1992) but only one has been approved by the FDA, recombinant tissue plasminogen activator (rt-PA). This agent can improve neurologic outcome if administered intravenously (IV) within the first 3 h after stroke onset (Chhabria and Torbey 2006). Because time is a critical variable for neuronal survival,

Address correspondence to: Christy K. Holland, Ph.D., Department of Biomedical Engineering, Colleges of Medicine and Engineering, Medical Science Building, Rm. 6167, University of Cincinnati, 231 Albert Sabin Way, Cincinnati, OH 45267-0586. E-mail: Christy.Holland@uc.edu

much effort has been directed toward accelerating the thrombolytic efficacy of rt-PA. However, this lytic agent has been shown to increase the risk of intracerebral hemorrhage (Lansberg et al. 2007).

There is significant interest in developing an adjunctive therapy that would improve rt-PA lytic efficacy and allow the reduction of the systemic rt-PA dose needed for treatment (Eggers 2006; Tsivgoulis and Alexandrov 2007). Intra-arterial (IA) infusion of thrombolytics have also been considered and enabled the use of lower doses of thrombolytics, with higher rates of recanalization compared with IV therapy, and hence lower rates of intracerebral hemorrhage (Shaltoni et al. 2007). Although IA-based techniques are attractive, they require the expertise of an experienced neurointerventionalist and they are time consuming (Dávalos 2005).

Ultrasound-enhanced thrombolysis has been demonstrated by several groups *in vitro* and *in vivo*, at clinically relevant settings (Eggers et al. 2003; Alexandrov et al. 2004). Improved thrombus degradation, drug transport and rt-PA binding to thrombi have been reported (Francis et al. 1995; Siddiqi et al. 1998; Alexandrov et al. 2004).

Furthermore, Molina et al. (2006) augmented the thrombolytic efficacy of rt-PA and 2.00-MHz transcranial Doppler ultrasound with an infusion of Levovist (Berlex Canada Inc., Lachine, Quebec) microbubbles, which resulted in a 17% increase of sustained recanalization. These investigators found that the microbubbles not only accelerated thrombolysis but also led to a more complete recanalization with a better short and long-term outcome.

An increased rate of cerebral hemorrhage was detected in a clinical study of transcranial ultrasound–enhanced rt-PA thrombolysis using 300-kHz, 700-mW/cm^2 (temporal average spatial peak intensity) pulsed ultrasound exposure, with a 5% duty cycle (PRF 100 Hz) (Daffertshofer et al. 2005). Using similar ultrasound parameters, Reinhard et al. (2006) performed perfusion magnetic resonance imaging and positron emission tomography studies in two patients post insonation and detected blood–brain barrier disruption. These observations emphasize the need to elucidate and delineate the complex interaction of ultrasound through and inside the skull.

Variability in the speed of sound in the different layers of the human skull contributes to effects of refraction and phase aberration of the intracranial field. This important property of the human skull was measured by Fry and Barger (1978). They identified a large range for the speed of sound (2570 to 3030 m/s) in the temporal bone. White et al. (1967) found that transducer positioning relative to the skull was also a very important factor for the penetration of ultrasound through the skull. These investigators determined that for optimal ultrasound penetration, the beam must be aligned 90 ± 5° to the temporal bone.

A better understanding of the interaction of ultrasound with the skull is essential to predict the acoustic pressure field within the brain. Knowledge about the shape of the ultrasound field in the brain is fundamental for ultrasound-enhanced or ultrasound-guided therapies. In this study, the penetration of pulsed ultrasound in the frequency range 0.12–2.00 MHz through the temporal bone was investigated experimentally. Both focused and unfocused ultrasound beams were tested and the intracranial field mapped at an estimated location of the MCA. This information is valuable not only for ultrasound-enhanced thrombolysis but also for other future therapeutic applications such as brain tissue ablation, blood–brain barrier opening for minimally-invasive drug delivery and for diagnostic imaging.

MATERIALS AND METHODS

Experimental apparatus

The beam patterns and skull transmission characteristics of three single-element ultrasound transducers with center frequencies of 0.12, 1.03 and 2.00 MHz were explored. A function generator (Agilent 33220A, Agilent Technology, Palo Alto, CA, USA) was used to drive both the 0.12 and 1.03-MHz transducers. The output of the function generator was connected to a power amplifier, (T&C Power Conversion Inc., Ultra 2021, 53 dB) or (Amplifier Research, 150LA, 47 dB) for the 0.12 and 1.03-MHz transducers, respectively. An impedance matching network (Sonic Concepts Inc., Seattle, WA, USA) was used to optimize the output of the 0.12-MHz transducer. The 2.00-MHz transducer was driven by a transcranial Doppler (TCD) system (DWL, EZ-Dop, Lindau, Germany).

All transducers were excited with a 40-cycle tone–burst signal, with a 6% duty cycle. The transducers were mounted on a manually controlled three-axis positioning system, with biplane angular adjustment for alignment with the temporal bone (Fig. 1). All transducers were driven such that the maximum peak-to-peak pressure amplitude in the free field was 0.29 ± 0.14 MPa. These pressure outputs were maintained for all experiments mapping the intracranial acoustic field because they allowed symmetric pressure waveforms (*i.e.*, linear regime). For each transducer, both axial and transverse beam profiles were measured in the free field (without a skull). The characteristics of each transducer are shown in Table 1.

Absolute calibration of the pressure output of the three transducers and beam profiling were performed with a Reson hydrophone (TC4038–1, Goleta, CA,

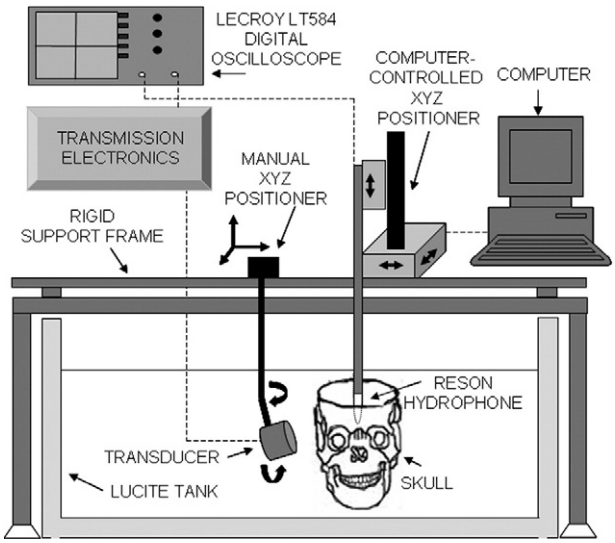

Fig. 1. Experimental setup.

USA) in a 97 × 57 × 54 cm^3 acrylic tank filled with 0.2 μm filtered, deionized, degassed water (20 to 22°C) and lined with an acoustic absorber (Aptflex F28, Precision Acoustics, Dorchester, England). The Reson hydrophone (1.3 mm active element) was cross-calibrated against a 0.5-mm bilaminar polyvinylidene difluoride hydrophone (Precision Acoustics Ltd.) at each frequency. The spatial averaging effects of the Reson hydrophone lead to less than an 8% underestimate of the peak-to-peak pressure output of the 2.00-MHz TCD transducer at its focus (Smith 1989).

A computer-controlled three-axis translation system (Velmex NF90 Series, Velmex, Inc. Bloomfield, NY, USA) provided 7.5-μm precision for moving the Reson hydrophone throughout the transmitted acoustic fields. This translation system is automated and controlled with a collection of visual interface programs written in LabView (National Instruments, Austin, TX, USA) on a desktop computer (Macintosh G5, Apple Computer, Inc., Cupertino, CA, USA). The entire setup (tank and micropositioning system) was placed on a vibration isolation table (IsoStation, Newport, CA, USA) to avoid unwanted vibrations of the hydrophone, skull and transducers. Measurements made with the hydrophone were digitized with an oscilloscope (Wave Runner LT584; LeCroy, Chestnut Ridge, NY, USA) and transferred to the same desktop computer.

Determination of the average MCA location relative to internal bony structures inside a human skull

The MCA is the laterally-directed terminal branch of the internal carotid artery, which courses horizontally between the basal surface of the brain and the skull base. In the clinical literature, the proximal basal horizontal segment of the MCA is frequently referred to as the M1 segment (Tanriover et al. 2003). This segment of the MCA, which is a common site for thromboembolic occlusion, extends from the internal carotid artery terminus (MCA origin) to the limen insula (M1 terminus) and has an average length of about 18 mm (Tanriover et al. 2003). This particular segment of the MCA was localized in 28 normal subjects by analyzing computerized tomography (CT) images after a protocol approved by the University of Cincinnati Institutional Review Board. Localization of the M1 was performed by determining the positions of the MCA origin and M1 terminus relative to fixed bony landmarks on the interior of the skull.

Twenty-eight consecutively performed head computerized tomographic angiograms (CTAs), in which the final clinical interpretation was normal, were selected for analysis. The CT studies included left (n = 25) and right (n = 3) MCAs from 17 men and 11 women, ages 17–83 (age ≤30, n = 8; age 30 to 60, n = 9; age >60, n = 11). CTAs were obtained on a General Electric Lightspeed Pro16 scanner (General Electric, Milwaukee, WI, USA) with 100 mL Isovue 370 (Bracco Diagnostics, Princeton, NJ, USA) injected at 3.5 mL/s through a 20-gauge peripheral IV catheter using bolus tracking. Coronal image planes separated by 1.25 mm were reconstructed from 2.5-mm slices, with a 0.625-mm overlap. Image analysis and related measurements were made using a SIENET MagicView workstation (Siemens, Erlangen, Germany). Based on a 512 × 512 pixel matrix with a 25-cm field-of-view, the spatial resolution in each image was approximately 0.5 mm. The antero-posterior (front–back) and craniocaudal (vertical) positions of the M1 origin and terminus were measured relative to a line connecting the tips of the anterior clinoid processes (ACPs, two bony protuberances on the upper part of the sphenoid bone lateral to the midline) in each subject (Fig. 2). The

Table 1. Ultrasound characteristics of the three transducers used in this study

Transducer center frequency (MHz)	−3 dB beam width (mm)	Focus/Rayleigh distance (mm)	Depth-of-field (mm)	Aperture (mm)	Type
0.12	24.0	92.2	76	61.4	Unfocused
1.03	6.0	81.3	60	25.4	Unfocused
2.00	2.5	35.1	46	14.0	Focused

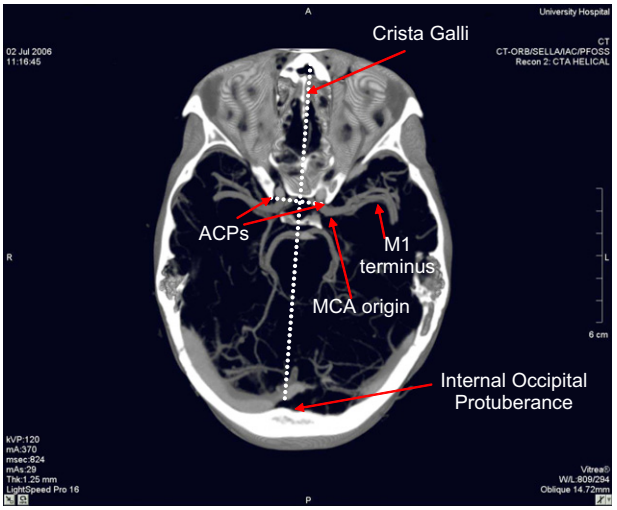

Fig. 2. Volume-rendered image of a normal patient. The thickness of the image is 14.7 mm, to allow the visualization of the bony landmarks and the vessels.

medial–lateral (left–right) position of each M1 origin and terminus was also measured in each subject relative to a line connecting the crista galli to the internal occipital protuberance (the two bone protuberances located at the front and back of the interior of the skull, respectively) (Fig. 2).

The average and standard deviation for each distance measurement were calculated. These coordinates were used to align the hydrophone at the estimated average position of the MCA origin inside the human skull specimens. In the following sections, the *X*, *Y* and *Z* coordinates pertain to the antero–posterior, craniocaudal and medial–lateral positioning, respectively. The origin of this *XYZ* coordinate system was chosen to be at the estimated average MCA origin.

Hydrophone alignment protocol within the skull

The average position of the MCA origin relative to the internal bony structures revealed in the CT imaging study was used in the protocol to align the Reson hydrophone within the human skull specimens. Five human skulls (provided by the Department of Cell and Cancer Biology at the University of Cincinnati College of Medicine) with the cranial skullcap removed were used for acoustic pressure field measurements in a plane encompassing the extent of the M1 from its origin to its terminus. The skullcap cut was above the temporal bone and parallel to the orbital shelf. Before each experiment, each skull was degassed in a vacuum chamber filled with deionized water for 40 min to minimize bubbles adhering to the skull during ultrasound insonation.

Each skull was mounted on a post, attached with clamps to the occipital bone well outside the ultrasound path. Each skull was positioned in the tank so that the ACPs were aligned horizontally and parallel to the *X* axis of the micropositioning motor. The hydrophone was carefully placed inside the skull at the tip of the right ACP. The distance separating the ACPs of the skull specimens was 22 ± 1.0 mm on average. Because the line connecting the crista galli to the internal occipital protuberance intersects the APC line in the middle, 11 mm was subtracted from the medial–lateral coordinates of the M1 origin and terminus. Using knowledge from the aforementioned CT study, the average location of the MCA origin relative to the right ACP was determined, and the acoustic center of the hydrophone, which is 4.2 mm from its tip, was moved to this location.

The acoustic window commonly used in transcranial examination of the MCA is the temporal bone, which is the thinnest portion of the skull, allowing maximum ultrasound penetration. Ten measurements of the temporal bone thickness for each of the five human skull specimens were made with a caliper (Cincinnati Precision Instruments, Inc., Cincinnati, OH, USA). Presented in Table 2 are the estimated average temporal bone thicknesses and standard deviations for each skull specimen. The transducers were positioned manually parallel to the temporal bone (11 ± 3° relative to the *Y* axis), above the zygomatic arch to optimize the penetration of the beam through the temporal bone. This angular adjustment of the transducers was done to maximize the hydrophone signal located at the MCA origin. The lower-frequency transducers, 0.12 MHz and 1.03 MHz, were positioned 40 ± 3 mm away from the temporal bone so that their natural focus was at the MCA origin. This placement avoided near-field interference and maximized the signal. For the 2.00-MHz transducer, an offset of at least 12 ± 3 mm between the transducer and the skull was maintained to mimic the tissue and muscle layers that normally cover the skull.

Using the computer-controlled micropositioning system, the hydrophone was scanned in the plane of the MCA across the skull medially, with a step increment of 1 mm in the *Z* (medial–lateral) direction and 1.0, 0.5 or 0.25 mm in the *X* (anteroposterior) direction for the 0.12, 1.03 and 2.00-MHz transducers, respectively. All field

Table 2. Estimated thickness of temporal bone and speed of sound in five skull specimens

Skull number	Temporal bone thickness (mm)	Arrival time difference (μs)	Speed of sound (m/s)
1	1.88 ± 0.4	0.64	3003.9
2	1.95 ± 0.4	0.20	1752.1
3	2.95 ± 0.4	0.16	1764.7
4	2.06 ± 0.4	0.76	3285.3
5	2.68 ± 0.4	0.88	2898.9

measurements were performed between the temporal bones, from the inside edge of the skull through the approximated MCA origin, to a point 100 mm intracranially. A volumetric scan encompassing the approximated location of the entire MCA segment was also performed (13 × 13 × 29 mm), with a step size of 1 mm. Scans were also performed close to the contralateral skull wall to investigate the possibility of constructive interference patterns near the bone. To allow for direct comparison, the skull was removed from the tank and a similar scan was run in the free field. For each scan, both the peak negative and the peak positive pressure values were recorded.

Data analysis

The processing of the intracranial ultrasound pressure data were performed off-line using MATLAB (The MathWorks Inc., Natick, MA, USA). The acoustic pressure field data were represented as a function of the peak-to-peak pressure. The peak-to-peak acoustic pressure at the estimated average location of the MCA origin, *i.e.*, at the coordinate (0, 0, 0), was extracted from each medial scan. The percent pressure reduction at the MCA origin relative to the free field was evaluated for the five human skull specimens at the three frequencies. The location and amplitude of the maximum peak-to-peak acoustic pressure inside each skull were extracted from the volumetric scan. The percent pressure reductions at this location relative to the free field were evaluated as well. The −3 dB beamwidth and depth-of-field were also evaluated in the skull, relative to the free field.

Measurement of speed of sound in the temporal bone

The speed of sound in the temporal bone was assessed at 21.0 ± 1°C by measuring the arrival time difference of the 1.03-MHz tone burst with the skull present *vs.* in the free field. Measurement of the speed of sound at 0.12 MHz was impossible because of the dimensions of the beam and the complexity of the path taken by the ultrasound. Measurement at 2.00 MHz was not performed because no trigger was provided by the TCD system used. Transmitted 1.03-MHz waveforms were recorded for each specimen with and without the presence of the skull. Each transmitted waveform was measured by averaging 100 transmitted pulses recorded by a digital oscilloscope at a 25-MHz sampling rate. The time delay between the initial positive maxima of the two averaged waveforms was determined with a time resolution of 40 ns for each specimen. The speed of sound, c_s, was calculated from the time–distance relation (Wear 2000; White et al. 2006)

$$c_s = \frac{d}{\frac{d}{c_w} - \Delta t}, \tag{1}$$

where d is the average thickness of the skull intercepted by the ultrasound beam, c_w is the speed of sound in the water and Δt is the arrival time difference with and without the skull present. The speed of sound in water was 1485.2 m/s for 21 ± 0.1°C (Kinsler et al. 1982).

Calculation of attenuation coefficient

To determine the attenuation coefficient of the temporal bone, three physical quantities were measured: the incident, reflected and transmitted ultrasound power for each skull specimen. The difference between the incident and the reflected power is defined as the ultrasound power penetrating the bone sample. The acoustic power across the beam was estimated from the plane wave formula:

$$\Pi = \frac{1}{2\rho c}\int_s |p|^2 \, dS, \tag{2}$$

where $|p|$ is the acoustic pressure amplitude, S is the cross-sectional area of the beam, ρ is the density of the water, and c is the speed of sound (Kinsler et al. 1982).

The transmitted power was determined from the volumetric transcranial field measurements described earlier. Because the ultrasound beam propagated obliquely, the sagittal plane, which encompassed most of the beam, was used for the transmitted power computation. To determine the incident and reflected powers, the field between the transducer and the skull specimens was measured. The skull and the transducers were positioned using the same alignment procedure described earlier. The Reson hydrophone was placed halfway between the transducer and the temporal bone along the transducer axis. The hydrophone was scanned in a plane perpendicular to the transducer axis with a 1-mm step size. Ten waveforms were recorded and averaged at each measurement point. At 1.03 and 2.00 MHz, the plane sizes were 31 × 31 mm^2 and 17 × 17 mm^2, respectively.

Thereafter, the skull was removed and the waveform data collection was repeated with the same step size. This data acquisition procedure was repeated for each of the five skulls. For each of the skulls, reflected waveforms were determined by subtracting the measured incident waveforms in the free field from the waveforms measured in the plane between the transducer and the temporal bone.

Incident, reflected and transmitted powers were estimated from eqn (2), with $|p|$ taken to be half the measured peak-to-peak acoustic pressure at each mesh point. The double integration was performed using the

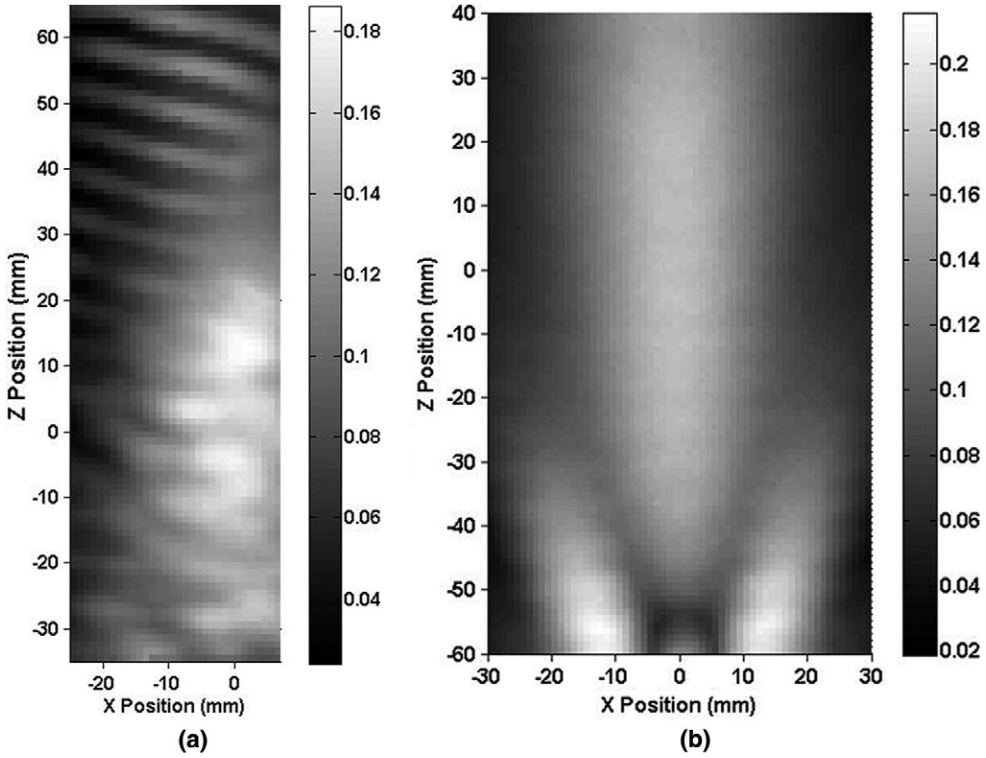

Fig. 3. Map of the peak-to-peak acoustic pressure (a) inside skull 1 and (b) in the free field insonified with an unfocused 0.12-MHz transducer.

MATLAB function, "*dblquad,*" with assistance from the functions, "*interp1*" or "*interp2,*" to interpolate data to the requisite mesh. The attenuation coefficient, α, was then derived from the ratio of transmitted and penetrating (incident minus reflected) powers as

$$\alpha = -\frac{1}{2L}\log\left(\frac{\Pi_{transmitted}}{\Pi_{incident} - \Pi_{reflected}}\right), \quad (3)$$

where the L is the skull thickness and $\Pi_{transmitted}$, $\Pi_{incident}$ and $\Pi_{reflected}$ are the ultrasound powers of the transmitted, incident and reflected fields, respectively.

The hydrophone scans of the intracranial acoustic beams were limited in extent because internal bony structures were present. Hence, pressure information on the edges of the beam were absent from the scans for the 1.03-MHz transducers, and even more at 0.12 MHz, partially because of the size of this single-element transducer. A correction factor was calculated for the transmitted power through each skull to account for this limitation for both frequencies. This correction factor was simply the ratio of the power measured in the free field at the natural focus (encompassing the entire beam) divided by the power measured in the free field at the natural focus within an equivalent limited area (as though the skull were present). Such a correction factor could not be calculated for the 0.12-MHz beam because a large portion of the beam extended to the internal bony structures of the skulls. Thus, attenuation coefficients were calculated for the 1.03 and 2.00-MHz beams only.

RESULTS

Average location of the MCA

The CT study enabled the localization of the average position of both the M1 origin and terminus relative to virtual intracranial axes defined by internal bony structures (a line connecting the ACPs and a line connecting the crista galli to the internal occipital protuberance). The average anteroposterior positions of the M1 origin and terminus and standard deviation of this measurement were 6.3 ± 2.7 mm and 1.2 ± 3.7 mm (anterior to the ACP line), respectively. The average craniocaudal positions were estimated to be 4.8 ± 2.3 mm and 8.5 ± 2.6 mm (above the APC line), respectively. The average medial–lateral positions of the M1 origin and terminus were 13.5 ± 2.3 mm and 33.9 ± 5.1 mm (from the line connecting the crista galli to the internal occipital protuberance), respectively. The distance between the M1 origin and terminus was estimated to be 21.84 ± 5.38 mm (mean ± standard deviation). The coordinate of the MCA origin was defined to be (0, 0, 0), and therefore the

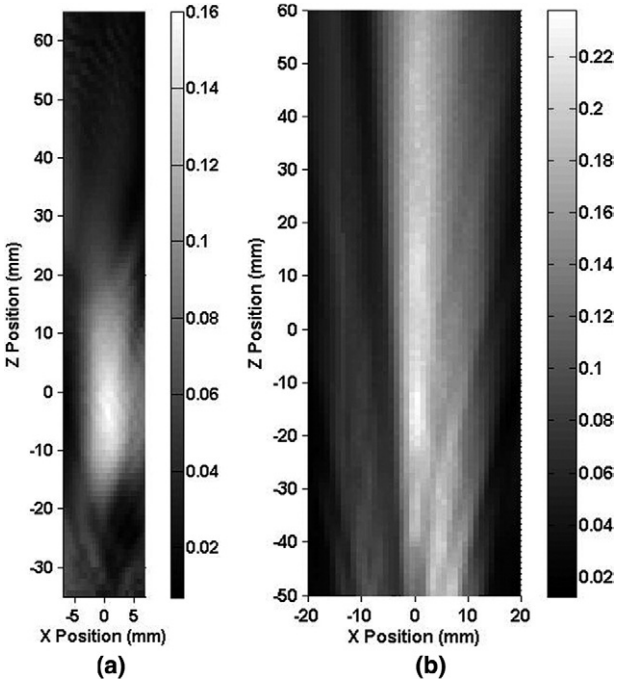

Fig. 4. Map of the peak-to-peak acoustic pressure (a) inside skull 1 and (b) in the free field insonified with an unfocused 1.0-MHz transducer.

M1 terminus location was (−5.1, 3.7, 20.4) in the *in vitro* study of the intracranial ultrasound field for all five skulls.

Intracranial ultrasound beam profiles

Shown in Fig. 3 are axial beam profiles of the 0.12-MHz transducer for skull 1 listed in Table 2. The intracranial and free field axial beam profiles are shown in Fig. 3, a and b, respectively. The *X*-axis corresponds to the anteroposterior direction and the *Z*-axis to the medial–lateral direction. The estimated location of the MCA origin was positioned at the (0, 0) coordinate in this scan. The black and white bar indicates the peak-to-peak ultrasound pressure in MPa. In these figures, the ultrasound propagates toward the positive *Z* direction. Note, in Fig. 3a, the pressure of intracranial bone structure limited the scans to 7 mm in the *X* direction. These structures prevented intracranial mapping of the entire beam for the 0.12-MHz transducer. The intracranial −3 dB beamwidth overlaps the estimated location of the MCA segment. The peak-to-peak acoustic pressure at the estimated MCA origin is 0.15 MPa and represents a 22.5% reduction in pressure from the free field maximum. The central part of the beam exhibits structure that may be caused by acoustic scattering from the ACPs and the orbital shelf inducing areas of constructive interference. Note also the constructive interference of the transmitted and reflected beam evident near the contralateral temporal bone. The general shape of the ultrasound beam profiles for the other skull specimens was similar. They also exhibited constructive interference patterns near the contralateral temporal bone.

Shown in Fig. 4 are the 1.03-MHz axial beam profiles obtained inside skull 1 and in the free field (no skull present). The shape of the intracranial ultrasound beam is an elongated oval in the *Z* (medial-lateral) direction. Because of the small beam size and transducer angle relative to the vertical (9 ± 1°), the ultrasound beam near the insonified temporal bone is not apparent at this elevation. At this frequency, because of the course of the MCA, the length of the M1 segment was not entirely within the intracranial −3 dB beamwidth. The central part of the beam does not seem to be as affected by the proximity of the intracranial structures as in the 0.12-MHz case. The peak-to-peak acoustic pressure achieved at the approximated MCA origin was 0.15 MPa and represents a 37.4% reduction in pressure from the free field maximum. Constructive interference patterns are present at this elevation but were even more obvious at

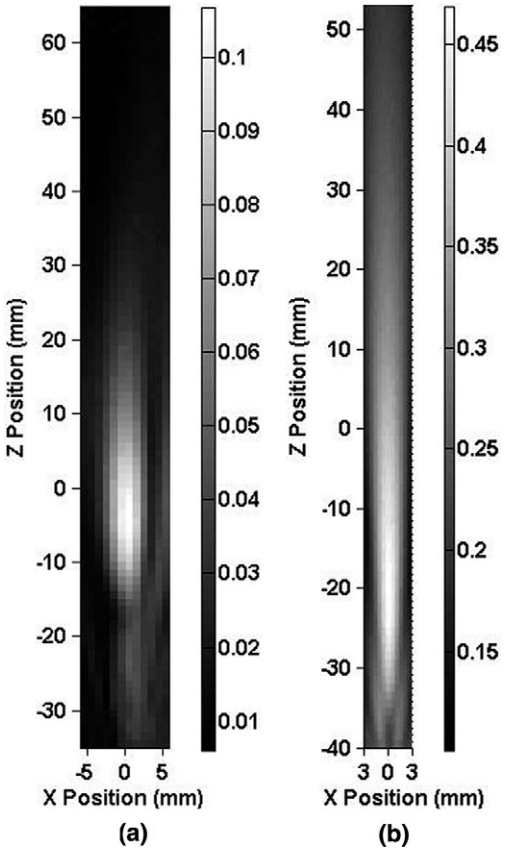

Fig. 5. Map of the peak-to-peak acoustic pressure (a) inside skull 1 and (b) in the free field insonified with a focused 2.0-MHz transducer.

Table 3. Percent pressure reduction at the MCA origin and at the location of the maximum peak-to-peak pressure relative to the free field. Also listed are metrics for the degree of ultrasound field aberration. The dashes indicate that no measurement was performed because of a severely distorted field (noncollimated beam)

Frequency (MHz)	Skull number	Percent pressure reduction at the MCA origin relative to the free field (%)	Percent pressure reduction at the position of maximum peak-to-peak pressure (%)	Relative position of maximum peak-to-peak pressure from the MCA origin (0,0,0) (mm)	Distance from the location of maximum peak-to-peak pressure from the MCA origin (mm)
0.12	1	22.5	4.4	(−2, −1, −5)	5.5
	2	41.9	14.2	(−3, 3, −22)	22.4
	3	45.5	15.5	(−4, 5, −17)	18.2
	4	23.0	0.9	(−6, −3, −20)	21.1
	5	32.8	8.0	(−3, 1, −19)	19.3
1.03	1	37.4	23.8	(0, −3, −21)	21.2
	2	91.6	—	—	—
	3	78.4	—	—	—
	4	59.5	42.7	(1, −2, −18)	18.1
	5	56.5	45.6	(−1, −4, −22)	22.4
2.00	1	80.4	69.0	(1, −4, −14)	14.6
	2	96.6	—	—	—
	3	92.1	—	—	—
	4	86.0	75.8	(1, −2, −19)	19.1
	5	77.1	76.4	(−1, −3, −20)	20.2

higher ones. Three of the five skulls studied exhibited the same beam pattern behavior, with collimated transcranial beams. However, the shape of the ultrasound beam inside two skulls (2 and 3) was strongly aberrated and was no longer coherent. Both of these skulls also exhibited the highest ultrasound pressure reduction (up to 96.6%).

Figure 5a shows an axial intracranial ultrasound beam profile using the 2.00-MHz focused TCD transducer at 7 ± 1° relative to the vertical. Within the skull, the ultrasound beam shape is oval and elongated in the *Z* direction in the same fashion as for the 1.03-MHz case. Note that for this focused 2.00-MHz beam, the entire length of the MCA is not within the intracranial −3 dB beamwidth. The peak-to-peak acoustic pressure at the origin is 0.08 MPa, which represents an 80.3% reduction in pressure from the free field maximum. No constructive interference patterns were present at this elevation but were present at higher ones, again because of the angle of the TCD transducer. Three of the five skulls exhibited similar field characteristics, whereas two of the skulls (2 and 3) severely attenuated ultrasound penetration through the temporal bone and reduced beam collimation.

Speed of sound in the temporal bone

The average tone burst arrival time differences for the five human skull specimens were derived experimentally at 1.03 MHz, and the results are shown in Table 2. Note that, although skull 3 had the thickest temporal bone, the arrival time difference measured for this specimen was the smallest (16 μs). The calculated speeds of sound in the temporal bone were also estimated and are included in Table 2. The speed of sound in the temporal bone exhibited a range from 1752.1–3285.3 m/s. Two of five specimens (2 and 3) had a relatively low measured speed of sound (<1800 m/s). The remaining skulls exhibited values almost double this value.

Percent pressure reduction

Presented in Table 3 are the percent pressure reductions at the estimated location of the MCA origin and at the position of maximum pressure relative to the free field, as well as the position of the maximum pressure and its distance from the MCA origin. The smallest and the largest percent pressure reduction at the MCA relative to the free field were at 0.12 and 2.00 MHz, respectively. At each frequency, skulls 2 and 3 presented the largest pressure reduction at the MCA. However, the pressure reductions for these two skulls at 0.12 MHz were smaller than those of all the skulls at 1.03 and 2.00 MHz (except skull 1 at 1.03 MHz). Similarly, the percent pressure reduction at the position of the maximum pressure relative to the free field was the smallest at 0.12 MHz for all the skulls. The percent pressure reduction at the position of the maximum pressure for skulls 2 and 3 at 0.12 MHz was 14.2% and 15.5%, respectively. These pressure reductions are smaller than those at 1.03 and 2.00 MHz for all the skulls. Note that at 0.12 MHz, skull 4 exhibited the lowest pressure reduction of the incident pressure wave. The displacements of the maximum peak-to-peak pressure amplitude relative to the approximated MCA origin are also reported in Table 3. For all frequencies, the largest displacements were in the medial–lateral direction. The maximum peak-to-peak pressure ampli-

Table 4. Average intracranial and free field ultrasound beam dimensions for 0.12, 1.03 and 2.00 MHz for skulls 1, 4 and 5 ($N = 3$)

Frequency (MHz)	Intracranial −3 dB beamwidth (mm)	Free field −3 dB beamwidth (mm)	Intracranial −3 dB depth-of-field (mm)	Free field −3 dB depth-of-field (mm)
0.12	18.8 ± 4.9	23.4 ± 1.1	41.0 ± 7.8	91.2 ± 11.1
1.03	7.2 ± 1.6	7.2 ± 1.0	24.0 ± 1.7	45.3 ± 3.0
2.00	3.6 ± 0.5	3.1 ± 0.6	18.0 ± 4.0	18.0 ± 1.5

tude generally shifted proximally toward the insonified temporal bone. For all frequencies, the shifts in the anteroposterior and the craniocaudal directions are negligible compared with those in the medial–lateral direction. Except for skull 1 at 0.12 MHz, which exhibited a displacement of 5.5 mm, all other skulls presented displacements between 18.1 and 22.4 mm.

Intracranial and free field beam dimensions

The average intracranial and free field beam dimensions are reported in Table 4. At 1.03 and 2.00 MHz, two of the skulls (2 and 3) were excluded from the beam dimension calculation because of the severe aberration exhibited. At 0.12 MHz, both the −3 dB beamwidth and depth-of-field were smaller intracranially than in the free field. However, the decrease in the depth-of-field was greater (~55%) than the decrease in the beamwidth (~20%). At 1.0 MHz, the −3 dB beamwidth did not change significantly in size. However, similar to the 0.12-MHz case, the intracranial −3 dB depth-of-field for the 1.03-MHz transducer was approximately a factor of two smaller than the free field. The beam dimensions of the 2.00-MHz TCD transducer did not change after penetrating the temporal bone.

Attenuation coefficient of the temporal bone

Table 5 lists the attenuation coefficient values derived from the incident transmitted and reflected acoustic powers for the five skulls at 1.03 and 2.00 MHz. The attenuation coefficient could not be calculated at 0.12 MHz because of the large extent of the intracranial beam in proximity to the location of bony structures. At 1.03 MHz, the measured attenuation coefficient varies from 154–713 Np/m. Note that skull 2 exhibited an attenuation coefficient three to five times higher than the other four skulls. At 2.00 MHz, the attenuation coefficient varied from 379–1210 Np/m. Skull 2 also has the highest attenuation coefficient of 1210 Np/m.

Table 5. Measured attenuation coefficients of the temporal bone in five human skulls at 1.03 and 2.00 MHz

Skull number	Temporal bone attenuation coefficient at 1.03 MHz (Np/m)	Temporal bone attenuation coefficient at 2.00 MHz (Np/m)
1	175 ± 37	558 ± 117
2	713 ± 143	1210 ± 242
3	216 ± 28	379 ± 49
4	255 ± 48	541 ± 103
5	154 ± 22	394 ± 55

DISCUSSION

This study provided some information regarding the average position of the M1 origin and terminus relative to intracranial bony structures in the human skull. These coordinates permitted the localization of the intracranial position of the MCA in our skull specimens, allowing measurements of the acoustic pressure in planes encompassing its estimated course. The average size of the M1 segment from its origin to its terminus was measured to be 21.84 ± 5.38 mm, which is within the range (10.14 to 29.32 mm) found in the anatomical literature (Tanriover et al. 2003).

Amplitude and phase distortions of the ultrasound beam were evident in the intracranial beam profiles obtained at 0.12 MHz. The large dimensions of the 0.12-MHz beam caused it to interact substantially with the bony structures adjacent to the M1 segment inside the cranium. This in turn also caused the presence of constructive interference as observed by other groups (White et al. 1978). Note particularly the interference pattern at the center of the beam (Fig. 3a), which probably occurred because of scattering from the ACPs (see Fig. 2). On the other hand, because of the large aperture of this transducer, the entire MCA segment was insonified, which is not the case for the smaller aperture transducers (1.03 and 2.00 MHz). For therapeutic strategies that rely on insonifying a thrombus within the MCA, broader beams that encompass the entire length of this intracranial artery may be advantageous.

Intracranial acoustic pressure profiles at both 1.03 and 2.00 MHz exhibited minimal distortion, except for skulls 2 and 3. Simulated intracranial fields by Clement and Hynynen (2002) affirmed that a sharp focal spot could be created at submegahertz frequencies but not at higher frequencies. We have shown that it is possible to obtain a focused beam at frequencies higher than 1.0

MHz. This might be attributed to the alignment procedure that enabled better penetration and less distortion when the transducer aperture is parallel to the temporal bone. In maximizing the signal received at the approximated location of the MCA origin by adjusting the angle of the transducer (Ringelstein et al. 1990), the ultrasound beam enters the plane of the MCA obliquely. This is clear in the scans performed at 1.03 and 2.00 MHz (Figs. 4a and 5a), where elongation in the Z (medial–lateral) direction is observed. However, the overall beam shape was uniform.

The profiles of two skulls (2 and 3 at 1.03 and 2.00 MHz, respectively) were strongly aberrated and demonstrated a complete lack of a collimated beam intracranially, as well as severe attenuation. All skulls were examined by an otolaryngology surgeon and were deemed to be morphologically and anatomically normal. The two skulls exhibiting higher ultrasound absorption had underdeveloped mastoid processes. Other *in vitro* and clinical studies have investigated some cases where the temporal bones were recalcitrant to the penetration of ultrasound (Kollár et al. 2004; Pfaffenberger et al. 2005). This lack of ultrasound penetration is referred to as temporal bone window insufficiency. Hence, the lack of ultrasound penetration in skulls 2 and 3 is probably attributable to an insufficient temporal bone window.

Indeed, many groups (Bruno et al. 1988; Marinoni et al. 1997; Postert et al. 1997; Dominguez-Roldan et al. 2004) have noted difficulties in clinical TCD studies *via* the temporal window. Insufficient penetration of TCD has been noted in elderly people, especially women and non-Caucasian groups (Itoh et al. 1993; Hoksbergen et al. 1999; Shambal et al. 2003). Hashimoto et al. (1992) reports an overall prevalence of temporal bone insufficiency in 29% of the global population, and 48%, if considering only women. A relationship exists between temporal bone window insufficiency and skull thickness. Jarquin-Valdivia et al. (2004) classified temporal bone window penetrability according to the quality of the TCD image obtained with 55 patients. Head CTs of the patients permitted the estimation of the temporal bone thickness. The percentage of patients presenting partial or no ultrasound penetration was 44% and correlated with the thickest temporal bones ($p \leq 0.0001$).

Among the five skulls in our study, skull 3 had the largest average temporal bone thickness (see Table 2). This skull also exhibited the largest percent pressure reduction and strongest beam aberration. Therefore, this skull likely depicts evidence of an insufficient temporal bone window. The temporal bone consists of three different layers of bone: the inner table (compact bone), the diploe (cancellous, sponge-like) and the outer table (compact bone). The central part of the bone (diploe) has a strong effect on the presence of temporal bone window insufficiency (Kollár et al. 2004).

Constructive and destructive interference was noted near the contralateral temporal bone at all frequencies. Using an optical technique, Azuma et al. (2005) observed similar acoustic patterns attributed to standing waves. We postulate that hemorrhages noted clinically in the contralateral, in clinical trials of ultrasound enhanced thrombolysis, might a result of such standing waves (Daffertshofer et al. 2005; Reinhard et al. 2006; Wilhelm-Schwenkmezger et al. 2007).

Measurements of the speed of sound in human temporal bone exhibited a large range of velocities (from 1752.1 m/s to 3285.3 ms) in the five skull specimens. Fry and Barger (1978) measured the speed of sound in each of three bone layers for three different temporal bone specimens at 1.00 MHz. The inner table had a range for speed of sound from 2810–3080 m/s. The speed of sound in the spongy diploe ranged from 2530–2860 m/s. The speed of sound in the outer table ranged from 2940–2960 m/s. The range for the speed of sound in the entire temporal bone was also reported to be from 2570–3030 m/s by Fry and Barger (1978). Goldman and Hueter (1955) and Goss et al. (1978) reported a speed of sound in skull of 3360 m/s at 0.8 MHz. Three of our skulls exhibited a speed of sound in the range found in the literature. Interestingly, the two skulls that demonstrated noncollimated intracranial ultrasound profiles also had the lowest measured speed of sound. It is possible that the large attenuation and beam distortions caused by these skulls affected the speed of sound measurements. More investigations are needed to determine if the speed of sound might be used as an index for the detection of insufficient temporal bone window. Insufficient temporal bone window is more common in older women primarily because of postmenopausal loss of mineral bone density (Ackerman et al. 1982; Itoh et al. 1993). Hence, the ultrasound penetrating through such temporal bones exhibits more scattering and results in less ultrasound penetration (White et al. 1978).

Results of the percent pressure reductions in Table 3 show that, at higher frequencies, the skull absorbs more ultrasound energy. However, two of the five skull specimens (2 and 3) exhibited the highest ultrasound absorption at each frequency. A solution to penetrating an insufficient temporal bone window with ultrasound might be the use of lower center frequencies, because a 41.9% and 45.5% reduction in pressure amplitude at the MCA origin were noted in these two skulls at 0.12 MHz. The percent pressure reduction at the position of the maximum pressure was even lower (14.2% and 15.4%).

The effect of skull-induced aberration on the maximum pressure location was shown to be dominantly in the medial–lateral direction (Table 3). Clement and

Hynynen (2002) also noted a shift in the focus of an intracranial steered-array beam by several millimeters from the predicted geometric location. This "targeting error" is probably caused by the variable thickness of the skull bone that introduces phase shifts, distorting the wave propagation.

Table 4 shows that the largest intracranial changes in the acoustic field dimension were in the depth-of-field at 0.12 and 1.03 MHz. On average, the depth-of-field was reduced by 50.20 mm and 21.33 mm for 0.12 and 1.03 MHz, respectively. No significant changes in the depth-of-field or beamwidth were measurable at 2.00 MHz after skull penetration. Note that this focused transducer was designed such that its focus was about 15.0 mm toward the temporal bone from the MCA origin. This places the MCA origin in the far field of the beam, where beam divergence is evident. Intracranial −3 dB beamwidths were very similar to those in the free field at all three frequencies. Beam dimensions of a 0.5-MHz transducer were quantified intracranially by Fry and Barger (1978), who similarly noted negligible reduction in the −6 dB beamwidth (not more than 0.4 mm).

Fry and Barger (1978) determined the attenuation coefficients of a single human temporal bone, both experimentally and numerically, for a range of frequencies from 0.25–2.00 MHz. The thickness of the temporal bone specimen was 6.0 mm and the diploe thickness was 2.5 mm. The measured attenuation values were 184 Np/m (10 dB) and 603 Np/m (32 dB) at 1.00 and 2.00 MHz, respectively. Theismann (1949) measured an attenuation coefficient of 151 Np/m in a human skull at 0.8 MHz. Hüter measured the average attenuation coefficients of temporal bones in 35 humans. The attenuation coefficients were 86, 167, 410 and 540 Np/m for 0.8 and 1.2, 1.8 and 2.25 MHz, respectively (Hüter 1952). These data can be interpolated linearly to provide attenuation coefficients of 121 Np/m and 467 Np/m at 1.0 and 2.0 MHz. The attenuation coefficients measured at 1.03 and 2.00 MHz in our study (Table 5) agree with these literature data, with the exception of one skull (2), which presented with an insufficient temporal bone window.

This technique is limited to specimens without insufficient temporal bone window because the calculation of the attenuation coefficient requires both sufficient transmitted power and penetrating (incident minus reflected) power. For these reasons, large errors in the measurement of attenuation are likely for those skulls exhibiting poor penetration of ultrasound through the temporal bone (skull 2). Also important might be the introduction of pockets of air within the temporal bone during the desiccation process for the preservation of human skulls. The degassing protocol followed before mapping the ultrasound field intracranially, however, should minimize the contribution of iatrogenic air to the measured attenuation values.

CONCLUSIONS

In this study, we provide a set of coordinates based on internal bony landmarks for the estimation of the location of the MCA origin and M1 terminus necessary, especially for careful characterization of a therapeutic ultrasound field in the brain. The intracranial acoustic pressure fields were measured at three different frequencies (0.12, 1.03 and 2.00 MHz) and depended crucially on the state of the temporal bone in each specimen. For those skulls not exhibiting insufficient temporal window, the beam characteristics were similar at all three frequencies. Beam characteristics such as shape, percent pressure reduction, depth-of-field and displacement of the focus or natural focus were measured. The lowest frequency tested, 0.12 MHz, permitted the highest penetration through the temporal bone, even for the two skulls where insufficient temporal bone was present. The most severe aberration was observed in these two specimens at 1.03 and 2.00 MHz. Transtemporal penetration of ultrasound tends to cause a significant shift toward the insonified temporal bone (up to 22.4 mm). Moreover, a relationship between the speed of sound in the temporal bone and the presence of an insufficient temporal window was present. This work will help in designing beamforming and center frequency characteristics for the development of therapeutic ultrasound systems in the brain.

Acknowledgements—This research was supported by the National Institutes of Health, grant number R01-NS047603. We appreciate the loan of the five skull specimens from Dr. Bruce Giffin in the Department of Cell and Cancer Biology in the College of Medicine at the University of Cincinnati. We are grateful for the expertise of Dr. Myles Pensak, Chair of the Otolaryngology Department at the University of Cincinnati, who examined the skull specimens.

REFERENCES

Ackerman LV, Buke MW, Boulos RS, Patel S. Computed measurements on computed tomograms of the head. Radiology 1982;143: 115–120.

Alexandrov AV, Molina CA, Grotta JC, Garami Z, Ford SR, Alvarez-Sabin J, Montaner J, Saqqur M, Demchuk AM, Moye LA, Hill MD, Wojner AW. Ultrasound-enhanced systemic thrombolysis for acute ischemic stroke. N Engl J Med 2004;351:2170–2178.

Azuma T, Kawabata K, Umemura S, Ogihara M, Kubota J, Sasaki A, Furuhata H. Bubble generaion by standing wave surrounding by cranium with transcranial ultrasound beam. Jpn J Appl Phys 2005; 44:4625–4630.

Berg-Dammer E, Mobius E, Nahser HC, Kuhne D. Local thrombolytic therapy for thromboembolic occlusion of the middle cerebral artery. Neurol Res 1992;14:164–166.

Bruno A, Biller J, Silvidi JA. A reason for failure to obtain transcranial Doppler flow signals. Hyperostosis of the skull. Stroke 1988;19: 274.

Chhabria N, Torbey MT. Acute ischemic stroke: Update on new therapies – and the implications for primary care. Consultant 2006; 46:1429–1433.

Clement GT, Hynynen K. Micro-receiver guided transcranial beam steering. IEEE Trans Ultrason Ferroelectr Freq Control 2002;49: 447–453.

Daffertshofer M, Gass A, Ringleb P, Sitzer M, Sliwka U, Els T, Sedlaczek O, Koroshetz WJ, Hennerici MG. Transcranial low-frequency ultrasound-mediated thrombolysis in brain ischemia: Increased risk of hemorrhage with combined ultrasound and tissue plasminogen activator—Results of a phase II clinical trial. Stroke 2005;36:1441–1446.

Dávalos A. Thrombolysis in acute ischemic stroke: Successes, failures, and new hopes. Cerebrovasc Dis 2005;20:135–139.

Dominguez-Roldan JM, Jimenez-Gonzalez PI, Garcia-Alfaro C, Rivera-Fernandez V, Hernandez-Hazanãs F. Diagnosis of brain death by transcranial Doppler sonography: Solutions for cases of difficult sonic windows. Transplant Proc 2004;36:2896–2897.

Eggers J, Koch B, Meyer K, König I, Scidel G. Effect of ultrasound on thrombolysis of middle cerebral artery occlusion. Ann Neurol 2003; 53:797–800.

Eggers J. Acute stroke: therapeutic transcranial color duplex sonography. Front Neurol Neurosci 2006;21:162–170.

Francis CW, Blinc A, Lee S, Cox C. Ultrasound accelerates transport of recombinant tissue plasminogen activator into clots. Ultrasound Med Biol 1995;21:419–424.

Fry FJ, Barger JE. Acoustical properties of the human skull. J Acoust Soc Am 1978;63:1576–1590.

Goldman DE, Hueter TF. Tabular data of the velocity and absorption of high frequency sound in mammalian tissues. J Acoust Soc Am 1955;28:35–37.

Goss SA, Johnston RL, Dunn F. Comprehensive compilation of empirical ultrasonic properties of mammalian tissues. J Acoust Soc Am 1978;64:423–457.

Hashimoto H, Etani H, Naka M, Kinoshita N, Nukada T. Assessment of the rate of successful transcranial Doppler recording through the temporal windows in Japanese with special reference to aging and sex. Jpn J Geriatrics 1992;29:119–122.

Hoksbergen AWJ, Legemate DA, Ubbink DT, Jacobs MJHM. Success rate of transcranial color-coded duplex ultrasonography in visualizing the basal cerebral arteries in vascular patients over 60 years of age. Stroke 1999;30:1450–1455.

Hüter TF. Messung der Ultraschallabsorption im menschlichen Schädelknochen und ihre Abhängigkeit von der Frequenz. Naturwissenschaften 1952;39:21–22.

Itoh T, Matsumoto M, Handa N, Maeda H, Hougaku H, Hashimoto H, Etani H, Tsukamoto Y, Kamada T. Rate of successful recording of blood flow signals in the middle cerebral artery using transcranial Doppler sonography. Stroke 1993;24:1192–1195.

Jarquin-Valdivia AA, McCartney J, Palestrant D, Johnston SC, Gress D. The thickness of the temporal squama and its implication for transcranial sonography. J Neuroimaging 2004;14:139–142.

Kinsler LE, Frey AR, Coppens AB and Sanders JV. The acoustic wave equation and simple solutions. In Fundamentals of Acoustics. New York: Wiley and Sons, Inc., 1982:98–123.

Kollár J, Schulte-Altedorneburg G, Sikula J, Fülesdi B, Ringelstein EB, Mehta V, Csiba L, Droste DW. Image quality of the temporal bone window examined by transcranial Doppler sonography and correlation with postmortem computed tomography measurements. Cerebrovasc Dis 2004;17:61–65.

Lansberg MG, Albers GW, Wijman CAC. Symptomatic intracerebral hemorrhage following thrombolytic therapy for acute ischemic stroke: A review of the risk factors. Cerebrovasc Dis 2007;24:1–10.

Marder VJ, Chute DJ, Starkman S, Abolian AM, Kidwell C, Liebeskind D, Ovbiagele B, Vinuela F, Duckwiler G, Jahan R, Vespa PM, Selco S, Rajajee V, Kim D, Sanossian N, Saver JL. Analysis of thrombi retrieved from cerebral arteries of patients with acute ischemic stroke. Stroke 2006;37:2086–2093.

Marinoni M, Ginanneschi A, Forleo P, Amaducci L. Technical limits in transcranial Doppler recording: Inadequate acoustic windows. Ultrasound Med Biol 1997;23:1275–1277.

Molina CA, Ribo M, Rubiera M, Montaner J, Santamarina E, Delgado-Mederos R, Arenillas JF, Huertas R, Purroy F, Delgado P, Alvarez-Sabín J. Microbubble administration accelerates clot lysis during continuous 2-MHz ultrasound monitoring in stroke patients treated with intravenous tissue plasminogen activator. Stroke 2006;37:425–429.

Pfaffenberger S, Devcic-Kuhar B, Kollmann C, Kasl SP, Kaun C, Speidl WS, Weiss TW, Demyanets S, Ullrich R, Sochor H, Wöber C, Zeitlhofer J, Huber K, Gröschl M, Benes E, Maurer G, Wojta J, Gottsauner-Wolf M. Can a commercial diagnostic ultrasound device accelerate thrombolysis? An in vitro skull model. Stroke 2005;36:124–128.

Postert T, Federlein J, Przuntek H, Büttner T. Insufficient and absent acoustic temporal bone window: Potential and limitations of transcranial contrast-enhanced color-coded sonography and contrast-enhanced power-based sonography. Ultrasound Med Biol 1997;23: 857–862.

Reinhard M, Hetzel A, Krüger S, Kretzer S, Talazko J, Ziyeh S, Weber J, Els T. Blood-brain barrier disruption by low-frequency ultrasound. Stroke 2006;37:1546–1548.

Ringelstein EB, Kahlscheuer B, Niggemeyer E, Otis SM. Transcranial Doppler sonography: Anatomical landmarks and normal velocity values. Ultrasound Med Biol 1990;16:745–761.

Shaltoni HM, Albright KC, Gonzales NR, Weir RU, Khaja AM, Sugg RM, Campbell MS 3rd, Cacayorin ED, Grotta JC, Noser EA. Is intra-arterial thrombolysis safe after full-dose intravenous recombinant tissue plasminogen activator for acute ischemic stroke? Stroke 2007;38:80–84.

Shambal S, Grehl H, Zierz S, Lindner A. Age dependence of Doppler parameters in the basal cerebral arteries evaluated by transcranial color-coded duplex sonography. Reference data from 290 volunteers. 2003;71:271–277.

Siddiqi F, Odrljin TM, Fay PJ, Cox C, Francis CW. Binding of tissue-plasminogen activator to fibrin: Effect of ultrasound. Blood 1998;91:2019–2025.

Smith RA. Are hydrophones of diameter 0.5 mm small enough to characterise diagnostic ultrasound equipment? Phys Med Biol 1989;34:1593–1607.

Tanriover N, Kawashima M, Rhoton Jr AL, Ulm AJ, Mericle RA. Microsurgical anatomy of the early branches of the middle cerebral artery: Morphometric analysis and classification with angiographic correlation. J Neurosurg 2003;98:1277–1290.

Theismann H, Pfander F. Uber die durchlassigkeit des knochens fur ultraschall. Strahlentherapie 1949;80:607–610.

Toumanidis ST. Cardiac sources of embolism in cerebral ischemia. Hellenic J Cardiol 1995;36:479–487.

Tsivgoulis G, Alexandrov AV. Ultrasound-enhanced thrombolysis in acute ischemic stroke: Potential, failures, and safety. Neurotherapeutics 2007;4:420–427.

Wear KA. The effects of frequency-dependent attenuation and dispersion on sound speed measurements: applications in human trabecular bone. IEEE Trans Ultrason Ferroelectr Freq Control 2000;47: 265–273.

White DN, Clark JM, White MN. Studies in ultrasonic echoencephalography. VII. General principles of recording information in ultrasonic B- and C-scanning and the effects of scatter, reflection and refraction by cadaver skull on this information. Med Biol Eng 1967;5:3–14.

White DN, Curry GR, Stevenson RJ. The acoustic characteristics of the skull. Ultrasound Med Biol 1978;4:225–252.

White PJ, Clement GT, Hynynen K. Longitudinal and shear mode ultrasound propagation in human skull bone. Ultrasound Med Biol 2006;32:1085–96.

Wilhelm-Schwenkmezger T, Pittermann P, Zajonz K, Kempski O, Dieterich M, Nedelmann M. Therapeutic application of 20-kHz transcranial ultrasound in an embolic middle cerebral artery occlusion model in rats: Safety concerns. Stroke 2007;38:1031–1035.

Zhil'tsova MN. [Hemodynamic indices in patients having sustained ischemic stroke and their dynamics during novocaine-electrophoresis treatment]. Klin Med (Mosk) 1965;43:115–118.